

Cryogenic electro-optic interconnect for superconducting devices

Amir Youssefi,^{1,*} Itay Shomroni,^{1,*} Yash J. Joshi,^{1,2} Nathan Bernier,¹

Anton Lukashchuk,¹ Philipp Uhrich,¹ Liu Qiu,¹ and Tobias J. Kippenberg^{1,†}

¹*Institute of Physics, École Polytechnique Fédérale de Lausanne (EPFL), CH-1015 Lausanne, Switzerland*

²*Indian Institute of Science Education and Research, Pune 411008, India*

Encoding information onto optical fields using electro-optical modulation is the backbone of modern telecommunication networks, offering vast bandwidth and low-loss transport via optical fibers [1]. For these reasons, optical fibers are also replacing electrical cables for short range communications within data centers [2]. Optical fibers exhibit more than 100-fold lower thermal conductivity than electrical copper cables, making optical interconnects based on electro-optical modulation an equally attractive candidate for interfacing superconducting quantum circuits [3–5] and hybrid superconducting devices [6]. Yet, little is known about optical modulation at cryogenic temperatures. Here we demonstrate a proof-of-principle cryogenic electro-optical interconnect, showing that currently employed Ti-doped lithium niobate phase modulators [7] are compatible with operation at 800 mK—below the typical operation temperature of conventional microwave amplifiers based on high electron mobility transistors (HEMTs) [8, 9]—and maintain their room temperature Pockels coefficient. We utilize cryogenic electro-optical modulation to perform coherent spectroscopy of a superconducting circuit optomechanical system, measuring optomechanically induced transparency (OMIT) [10–13]. In addition, we perform incoherent spectroscopy by encoding thermomechanical sidebands from the microwave domain onto an optical signal processed at room temperature. Although the currently achieved noise figure is significantly higher than that of a typical HEMT, the reduced operating temperature inherently allows lower added noise. Further noise reduction should be attainable by harnessing recent advances in integrated modulators [14, 15], by increasing the modulator length, or by using materials with a higher electro-optic coefficient [16, 17]. Our work highlights the potential of lithium niobate modulators for massively parallel readout for emerging quantum computing [3–6] or cryogenic classical computing [18] platforms.

Optical modulators are ubiquitous in our information society and encode electrical signals in optical carriers

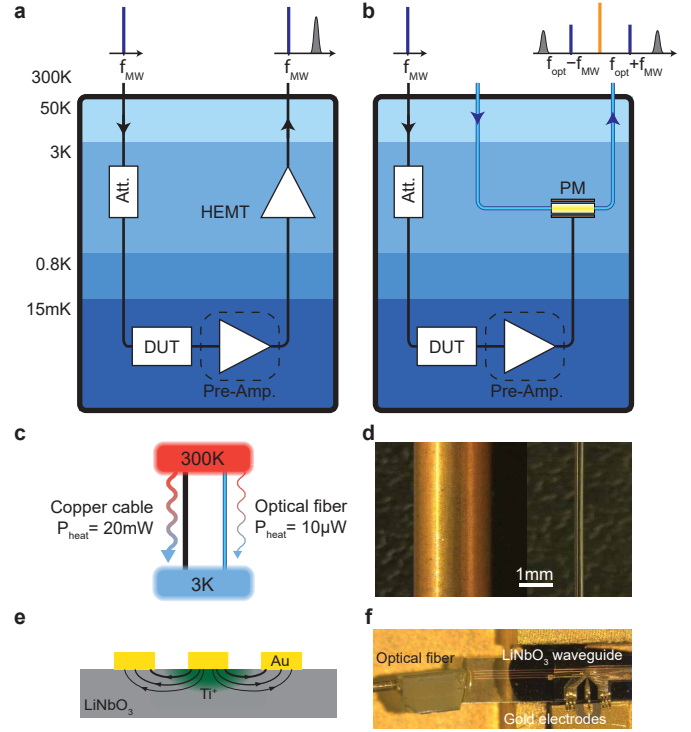


FIG. 1. Principle of a cryogenic electro-optical interconnect for readout of superconducting devices. **a**, Simplified schematic of a conventional readout of a device under test (DUT) in a dilution fridge using a HEMT amplifier. The dashed box indicates an optional quantum-limited preamplifier not used in this work. The devices are interrogated by input microwave signals that are attenuated to reduce thermal noise, and amplified using an HEMT amplifier at 3 K. **b**, Principle of a cryogenic electro-optic readout scheme using an electro-optic phase modulator. The DUT is interrogated using the same microwave input line, but the microwave signals are converted to the optical domain at 3 K, reducing thermal load. **c**, Conducted heat through a conventional copper coaxial cable and optical fiber between room temperature and 3 K. **d**, Picture of a copper coaxial cable and optical fiber. **e**, Schematic cross-section of a Z-cut LiNbO₃ telecommunication phase modulator. **f**, Microscope photo of a phase modulator connected to optical fiber.

that can be transported over fiber. Initially only used for long-haul communications, optical fiber links are now also replacing electrical copper cables for short range communications within data centers [19–21]. This is motivated by the high power consumption of electrical interconnects that spurred the development of optical in-

* These authors contributed equally.

† tobias.kippenberg@epfl.ch

terconnects based on silicon photonics [20]. Such interconnects may also be used in the future for on-board chip-to-chip communication [22, 23].

A similar challenge is foreseeable in superconducting quantum circuits. Recent advances in superconducting quantum circuits [3–5] have highlighted the potential associated with scaling superconducting qubit technology [24]. Currently, significant efforts are underway to scale the number of qubits. As a result, one of the challenges that future progress in superconducting circuits will face is to massively increase the number of microwave control and readout lines while preserving the base temperature and protecting qubits from thermal noise. Figure 1a shows a prototypical measurement chain of a single superconducting device-under-test (DUT) that operates at the 15 mK stage of a dilution refrigerator. Copper coaxial cables are used to transmit amplified signals to the room temperature as well as feeding MW control signals to the cold stages of the fridge. To read out GHz microwave signals, a high electron mobility transistor (HEMT) amplifier with low-added-noise [$n_{\text{add}} = \mathcal{O}(10)$ quanta/(s · Hz)] is typically employed that operates at the 3 K stage and amplifies the DUT output signal for further processing outside the cryostat. Although HEMTs are not quantum-limited [8, 9], the development of Josephson junction-based pre-amplifiers [25–28] that operate at the 15 mK stage have allowed near-quantum-limited microwave amplification. In addition, the input copper lines, that extend from room temperature down to 3 K, necessitate the use of cold attenuators to prevent room temperature thermal noise from reaching the devices at base temperature (Fig. 1a). This leads to significant heat load, which is exacerbated by the high thermal conductivity of the cables.

In contrast, the thermal conductivity of silica, $k_{\text{SiO}_2} = \mathcal{O}(1 \text{ W m}^{-1} \text{ K}^{-1})$, makes optical fibers excellent thermal insulators compared to copper cables, with $k_{\text{Cu}} = \mathcal{O}(100 \text{ W m}^{-1} \text{ K}^{-1})$. Optical fibers additionally exhibit ultralow-loss signal propagation ($\sim 0.2 \text{ dB/km}$) compared to copper lines. Optical fibers could therefore provide a solution to scaling the number drive lines (Fig. 1c) without the concomitant heating. For this approach, a critical component are modulators which convert input microwave signals to the optical domain that are compatible with low temperature operation and are sufficiently efficient to ensure low noise (quantum-limited) transduction of microwave to optical signals. Indeed, substantial efforts are underway to create quantum-coherent interfaces between the microwave and optical domains. To date, quantum coherent conversion schemes based on piezoelectromechanical [29, 30], magneto-optical [31], and optomechanical [32–34] coupling have been developed. In addition, schemes based on cavity electro-optics [35] have been demonstrated using bulk [36, 37], and integrated [38] microwave cavities coupled via the Pockels effect to an optical cavity mode. Yet, all these schemes have in common that they transduce *narrow-band* microwave signals to the optical domain. While this ability is criti-

cal for future quantum networks, an optical replacement for the currently employed HEMT amplifiers may be required for scaling control lines. One route is therefore to use *broadband* optical modulators as already used today in telecommunication networks.

Here we explore this potential and replace the HEMT amplifier with a LiNbO₃-based optical phase modulator (PM), the workhorse of modulator technology, in order to directly transduce the DUT microwave output signal onto sidebands around the optical carrier field (Fig. 1b), detectable using standard homodyne or heterodyne detection schemes at ambient temperatures. To illustrate the principle of the readout, we consider the operating principle of a PM. Optical PMs are based on the Pockels effect (Fig. 1e) and induce a phase shift on the input optical field $E_{\text{in}}(t)$, proportional to the voltage $V(t)$ applied on the input microwave port of the device,

$$E_{\text{out}}(t) = E_{\text{in}}(t)e^{-i\pi V(t)/V_{\pi}} \approx E_{\text{in}}(t)[1 - i\pi V(t)/V_{\pi}], \quad (1)$$

where the half-voltage V_{π} is the voltage at which the phase shift is π , and typical $V(t) \ll V_{\pi}$ is assumed. The relation between microwave (field operator \hat{b}) and optical (field operator \hat{a}) photon flux spectral densities [39], \bar{S}_{bb} and \bar{S}_{aa} respectively, can be written as (see Appendix)

$$\bar{S}_{aa}[\omega_{\text{opt}} \pm \omega_{\text{MW}}] = G \times (\bar{S}_{bb}[\omega_{\text{MW}}] + n_{\text{add}}) \quad (2)$$

where ω_{MW} and ω_{opt} are the microwave signal and optical carrier frequencies, n_{add} is the added noise of the transducer (referred back to the input), and the transduction gain G is the number of transduced optical photons per microwave input photon, is given by (see Appendix):

$$G = P_{\text{opt}} \frac{\omega_{\text{MW}}}{\omega_{\text{opt}}} \frac{\pi^2 Z_0}{2V_{\pi}^2} \quad (3)$$

where P_{opt} is the power of the optical carrier at the output of the PM, and Z_0 the input microwave impedance of the PM. In this experiment, we employ a *z*-cut traveling wave Ti-doped LiNbO₃ PM with specified bandwidth of 10 GHz and $V_{\pi} = 7.5 \text{ V}$ at 10 GHz. We use a 1555 nm fiber laser as the optical source. The typical input power to the fridge is 25 mW, and the total optical efficiency between the fridge input and output is 13%.

Previous works investigated the temperature dependence of the electro-optic coefficient and refractive index of congruent LiNbO₃ at low frequencies down to 7 K [40]. Commercial *x*-cut LN modulators were also tested down to 10 K, showing a slight change in V_{π} from its room temperature value [41, 42]. Ref. [43] discusses the behavior of LN modulators with superconducting electrodes down to 4 K. To date, however, such modulators have not been used in a dilution refrigerator to directly read out a superconducting device.

Characterization. To characterize the electro-optic behavior of the device at cryogenic temperatures, we mount the PM on the 800 mK flange of the dilution fridge. We directly drive the MW port of the PM at

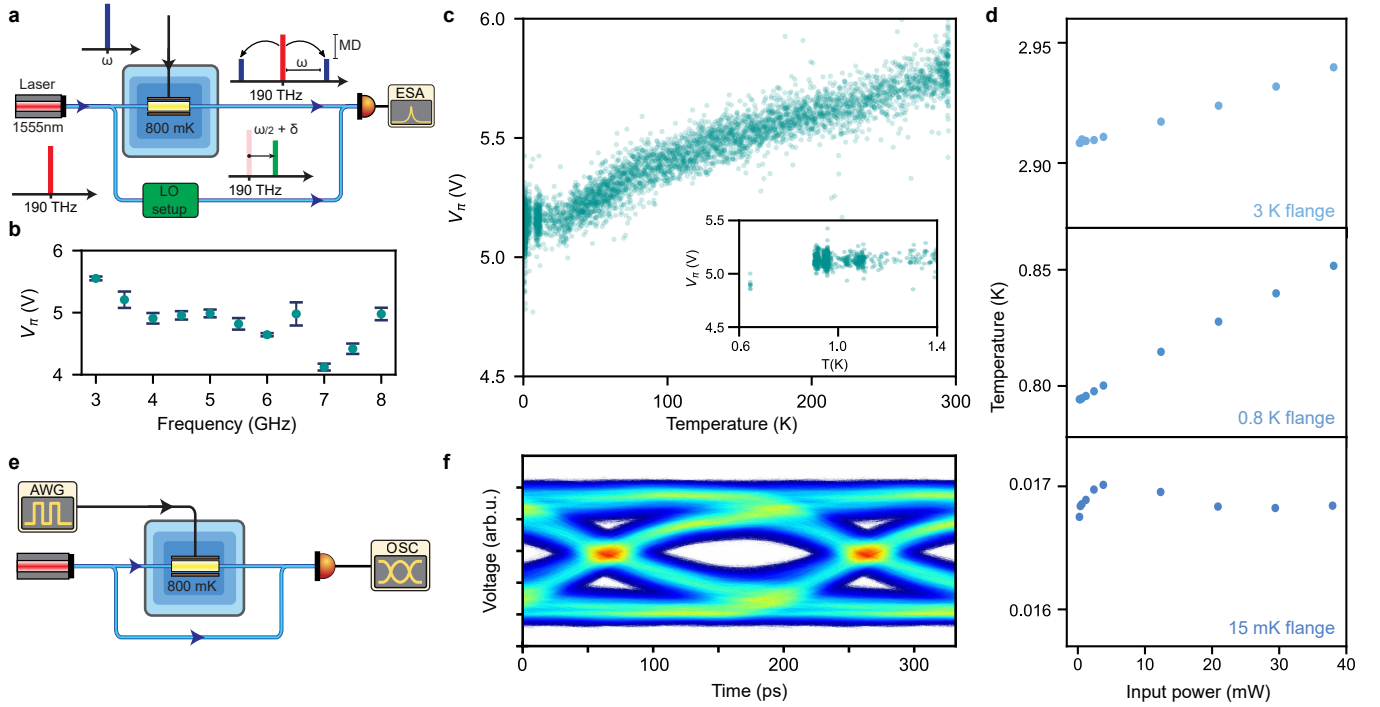


FIG. 2. **Cryogenic characterization of a LiNbO₃ phase modulator.** **a**, Experimental setup for low temperature characterization of the phase modulator. **b**, plot of V_π vs. frequency at 800 mK. **c**, Characterization of V_π at 5 GHz vs. temperature from room temperature to 800 mK. **d**, Measurement of heating due to optical dissipation when the phase modulator is mounted on the 800 mK flange. Plot of the steady state temperature vs. input laser power of the 3 K, 800 mK, and 15 mK flanges. **e**, Experimental setup for phase shift keying detection. RF signal from waveform generator is directly applied on a phase modulator. After homodyne detection the electrical signal is recorded on a fast oscilloscope. **f**, Eye-diagram of an optical signal phase-modulated at a rate of 5 GBaud, the bit error rate is 5×10^{-5} .

frequency ω_{MW} using a microwave source outside the fridge, generating sidebands around the optical carrier frequency (Fig. 2a). The half-voltage V_π is determined from the modulation depth MD, defined as the ratio of the power in one of sidebands to the power in the carrier,

$$V_\pi = \pi \sqrt{\frac{Z_0 P_{\text{MW}}}{2 \text{MD}}}, \quad (4)$$

where P_{MW} is the power at the MW input port of the PM. We measure MD by beating the output optical signal with a local oscillator (LO) with frequency $\omega_{\text{opt}} + \omega_{\text{MW}}/2 + \delta$, generating two closely-spaced beatnotes at $\omega_{\text{MW}}/2 \pm \delta$, due to the carrier and the high-frequency sideband. Using Eq. (4) we extract V_π by sweeping MW power and measuring MD. Figure 2c shows V_π at 5 GHz monitored as the fridge is cooled down from room temperature to 800 mK, and Fig. 2b shows V_π at different frequencies at 800 mK. Importantly, V_π does not change substantially from the room temperature value.

To investigate the effect of heating caused by optical dissipation in the PM, we measured the steady state temperature of different flanges of the dilution fridge when the PM is mounted on 800 mK flange. As seen in Fig. 2d, we did not observe an appreciable temperature change with input optical power as high as 50 mW, showing the

potential of operating at this temperature—a considerable advantage over HEMTs, which are typically operated at 3 K and are therefore susceptible to additional thermal noise.

To further assess the performance of the PM at 800 mK, we also performed a basic telecommunication experiment shown in Fig. 2e. An arbitrary waveform generator (AWG) directly drives the PM with a pseudo-random bit sequence at a rate of 5 GBaud/s. We beat the optical phase-modulated carrier output with its reference arm, where the transmission of the effective Mach-Zehnder interferometer is adjusted by tuning the laser frequency, and detect the electrical signal on the oscilloscope. Figure 2f shows an eye diagram obtained from the traces of 8×10^5 samples, leading to an upper bound on the bit error-rate of 5×10^{-5} with 95% confidence level [44, 45]. These measurements clearly demonstrate that the cryogenic modulator still functions at 800 mK.

Coherent measurements. Having established the cryogenic modulation properties, we next carry out a cryogenic interconnect experiment, where the MW output of a DUT is read out optically. As an example system we employ a superconducting electromechanical device in the form of a mechanically-compliant vacuum gap capacitor parametrically coupled to a superconducting microwave resonator (Fig. 3a–e). These devices have been

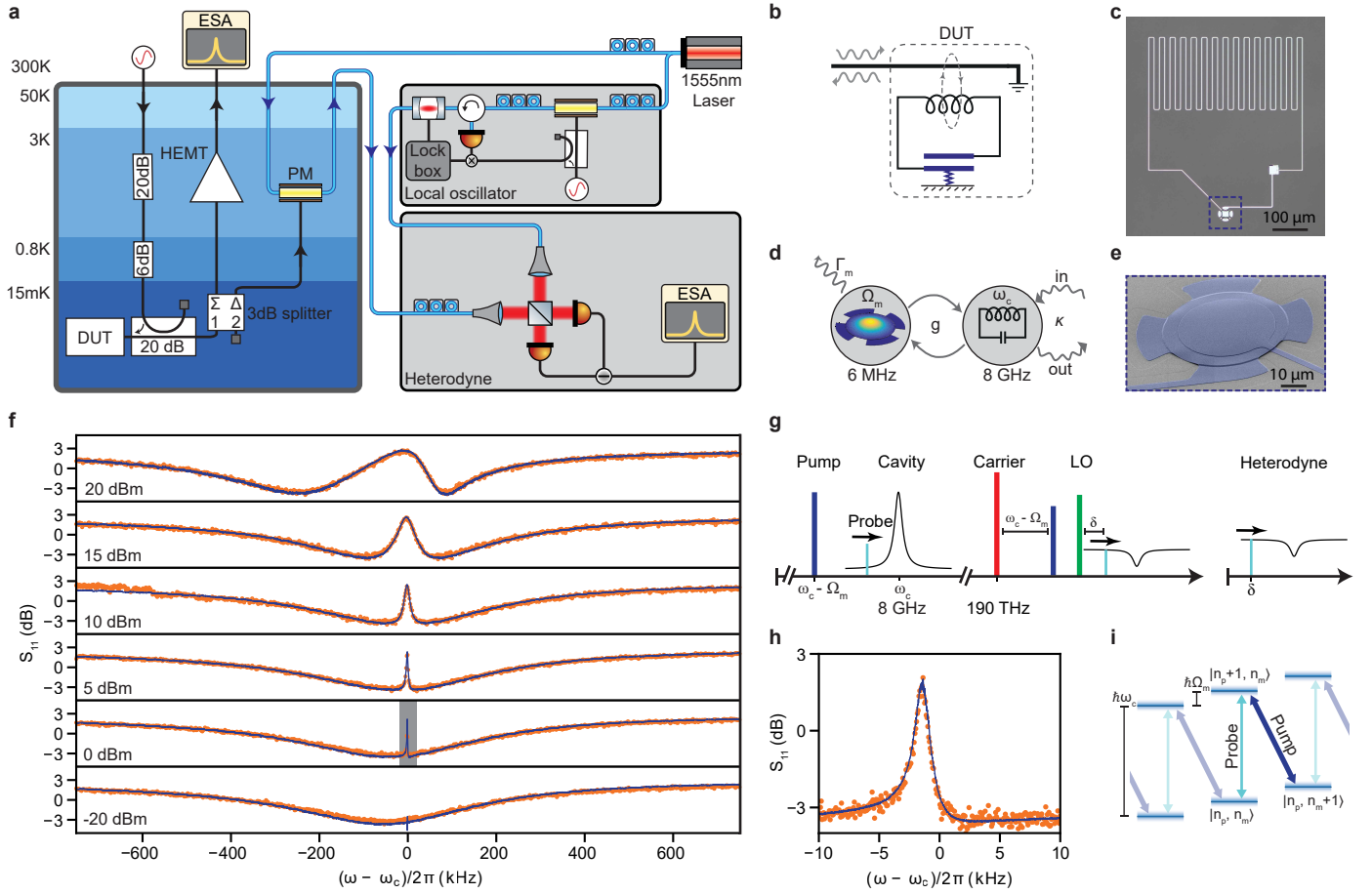


FIG. 3. Electro-optic readout via coherent spectroscopy of a superconducting electromechanical system. **a**, Experimental setup. Left: dilution fridge, right: optical setup. **b**, Electromechanical system used as a DUT. **c**, optical micrograph of the *LC* resonator. **d**, Modal diagram of the electromechanical system. **e**, scanning electron micrograph of the mechanically compliant capacitor. **f**, coherent measurement of the electromechanical resonance for increasing MW pump powers of $(-20, 0, 5, 10, 15, 20)$ dBm at the source, from bottom to top respectively. The probe power is -20 dBm at the source. By increasing the pump power, the optomechanically induced transparency window emerges, and at stronger pump powers the modes get strongly coupled, leading to an avoided crossing effect. Blue lines correspond to HEMT readout and orange dots to optical readout. **g**, the frequency scheme for microwave tones, optical tones, and measured signal after the heterodyne. **h**, high resolution measurement of the transparency window highlighted in **f** with the gray box. **i**, level scheme of the optomechanical system. The pump tone is tuned close to red sideband transitions, in which a mechanical excitation quantum is annihilated (mechanical occupation $n_m \rightarrow n_m - 1$) when a photon is added to the cavity (optical occupation $n_p \rightarrow n_p + 1$), therefore coupling the corresponding energy eigenstates. The probe tone probes reflection in which the mechanical oscillator occupation is unchanged. The pump tone modifies the response of the cavity and creates a transparency window appears on resonance (OMIT).

employed in a range of quantum electromechanical experiments, such as cooling the mechanical resonator to its quantum ground state [46], strong coupling between mechanical and microwave modes [13], squeezing of mechanical motion [47], and demonstration of the quantum entanglement in the mechanical motion [48, 49], as well as implementing mechanically mediated tunable microwave non-reciprocity [50] and quantum reservoir engineering [51]. The microwave resonance (frequency $\omega_c \simeq 2\pi \times 8.2$ GHz and linewidth $\kappa \simeq 2\pi \times 3$ MHz) is coupled to the mechanical resonance (frequency $\Omega_m \simeq 2\pi \times 6$ MHz and linewidth $\Gamma_m \simeq 2\pi \times 10$ Hz) of the capacitor via electromechanical coupling [52] (Fig. 3d). The

electromechanical coupling rate is $g = g_0 \sqrt{\bar{n}_{\text{cav}}}$, where $g_0 \simeq 2\pi \times 150$ Hz and \bar{n}_{cav} is intra-cavity MW photon number, proportional to the MW pump power. The system is inductively coupled to a microwave feed-line, enabling us to pump and read out the microwave mode in reflection.

To demonstrate the electro-optical readout technique, we perform two-tone spectroscopy and measure optomechanically induced transparency (OMIT) [10–12] (Fig. 3i) on the electromechanical sample, by applying a MW pump tone on the lower motional sideband (red-detuned by Ω_m from the cavity resonance) and sweeping a second probe tone across the resonance. The strong pump

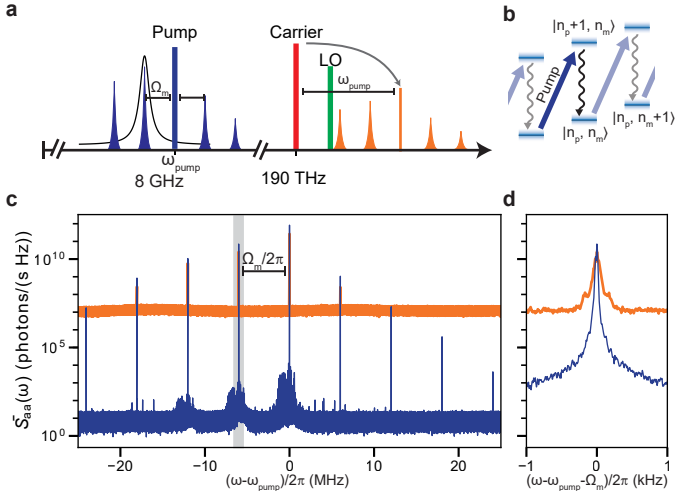


FIG. 4. Electro-optic readout via incoherent spectroscopy of a superconducting electromechanical system. **a**, Frequency-domain picture: a microwave tone pumps the electromechanical system on the upper motional sideband, inducing a parametric instability and generating mechanical sidebands equally spaced around the tone by the mechanical resonance frequency Ω_m . The phase modulator transfers the microwave spectrum on the optical signal, which is subsequently mixed with a local oscillator (LO) and detected via heterodyne detection. **b**, Level scheme showing electromechanically induced parametric instability. A blue-detuned pump photon scatters into an on resonance photon and generates a phonon in the mechanical oscillator and causes anti-damping. At pump power above a certain threshold induces instability in the mechanical oscillator. **c**, Measured power spectral densities of the microwave pump (central peak) and mechanical sidebands detected by the HEMT (blue) and optical (orange) readouts. **d**, Power spectral densities of the on-resonance mechanical sideband highlighted in **c** with gray shading.

damps the mechanical motion, resulting in a wider effective mechanical linewidth, $\Gamma_{\text{eff}} = \Gamma_m + 4g^2/\kappa$. The microwave pump modifies the cavity response due to the electromechanical coupling, resulting in a transparency window that appears on resonance of width Γ_{eff} , which we observe by the probe (Fig. 3g). We performed an OMIT experiment for different pump powers and observed the mechanical resonance via the transparency feature. In order to electro-optically read out the coherent response, the optical output is detected in a balanced heterodyne detector, using a frequency-shifted local oscillator (Fig. 3g). To compare the optical and HEMT readouts, the reflected signal is split and measured simultaneously using both techniques (Fig. 3a). Figure 3f shows the OMIT results, with excellent agreement between the optical and HEMT readouts. At high pump powers, when $g \sim \kappa$, we observe mode splitting as a result of strong coupling and mode-hybridization between the mechanical and microwave modes [13].

Incoherent measurement. Next, we investigated incoherent signal detection using the optical readout and

measured the power spectral density of a signal emitted by the DUT. For this, we drive the mechanical oscillator into the self-oscillation regime by pumping the system on its upper motional sideband, $\omega_{\text{pump}} = \omega_c + \Omega_m$, inducing a parametric instability [52–55]. The output microwave spectrum features strong sidebands around the microwave pump, at integer multiples of the mechanical frequency (Fig. 4a,b). Using our optical readout, we can detect these mechanical signals, and compare the results with the simultaneously-measured HEMT output (Fig. 4c,d) in order to compute the transduction gain G . We first use the independently characterized added noise of the HEMT amplifier (referred to the input), $n_{\text{add}}^{\text{HEMT}} \simeq 8 \text{ quanta}/(\text{s} \cdot \text{Hz})$ to calibrate the power spectral density measured in the HEMT branch. We similarly use the optical shot noise floor to calibrate the optical output. We then use the MW input, obtained from the HEMT calibration, and the optical output to estimate the transduction gain, $G = 0.9 \times 10^{-7}$ [Eq. (2)], in good agreement with the theoretical value $G^{\text{theory}} = 3.5 \times 10^{-7}$ obtained from Eq. (3) using the measured output optical power in the carrier, $P_{\text{opt}} = 1.1 \text{ mW}$ (optical efficiency of 5%, including losses in heterodyne detection setup). We note that the frequency widening of the optically detected sidebands, observed in Fig. 4d, is due to fluctuations in the LO frequency, caused by the limited bandwidth of the locking setup in conjunction with using a minimal resolution bandwidth (RBW) of 1 Hz in the spectrum measurement. The integrated sideband power, however, is conserved. Improving the LO locking setup can reduce this effect.

The added noise in the transduction process is (see Appendix)

$$n_{\text{add}} = \frac{1}{2G} + n_{\text{th}}^{\text{MW}} + \frac{1}{2}, \quad (5)$$

where $n_{\text{th}}^{\text{MW}}$ is the average occupation of the thermal photonic bath due to MW fields. As shown the noise floor of the optical measurement is 60 dB above the HEMT readout. This is due to the very small gain factor $G \sim 10^{-7}$, caused by the large V_{π} and the limited optical power. In the Appendix we discuss a quantum mechanical model of the phase modulator and show that when the gain $G > 1$, e.g., $V_{\pi} \sim 10 \text{ mV}$ and $P_{\text{opt}} \sim 10 \text{ mW}$, the device can operate as a phase insensitive near-quantum-limited amplifier ($n_{\text{add}} = 2 \text{ quanta}/(\text{s} \cdot \text{Hz})$ at 800 mK). Half-voltages lower by two orders of magnitudes and optical efficiencies exceeding 90% have been recently demonstrated exploiting integrated modulators with closer electrodes, and longer devices [56, 57], and new materials such as BaTiO₃ [16, 17, 58]. Eq. (3) shows that achieving same efficiency as a HEMT ($G \sim 5 \times 10^{-2}$) in improved devices is feasible in the near future.

It is worth mentioning that many experiments utilize a near-quantum-limited pre-amplifier at the 15 mK stage (Fig. 1a,b). In this case, the noise added in the second amplification stage, referred to the input, is $\sim (G_{\text{PA}} G)^{-1}$ (see Appendix), where $G_{\text{PA}} = \mathcal{O}(10^3)$ is the pre-amplifier

gain [25–28]. Thus, $G \gtrsim G_{\text{PA}}^{-1}$ suffices to preserve near-quantum-limited transduction (See Appendix). In this case, the compatibility of the electro-optic transducer with operation at 800 mK (as opposed to 3 K for the HEMT) is a great advantage because of the reduced thermal noise.

Conclusions. We have demonstrated the viability of LiNbO₃ devices, currently-employed in the telecommunication market, as components in cryogenic platforms used in superconducting quantum technologies, in particular by showing operation at sub-Kelvin temperatures with negligible laser induced heating. By interfacing a commercial PM to a circuit-electromechanical system that was previously used to perform quantum experiments, we quantified the gap between conventional microwave amplifiers and the electro-optical alternative. It is feasible that this gap be closed in the near future, by improved devices with lower V_π , resulting in a quantum-limited broadband microwave-to-optical interconnect.

Appendix: Quantum mechanical model for a phase modulator

In the following, we derive a simple quantum description of the phase modulator to establish the quantum limits in transducing the input microwaves. The central assumption is that the linear regime stays valid, for sufficiently low input microwave powers. As such, the scattering equations linking inputs to output should be identical in both quantum and classical cases. We can use the known classical regime as a starting point, with the output optical field amplitude \hat{a}_{out} expressed as a function of the input optical field \hat{a}_{in} as

$$\hat{a}_{\text{out}} = e^{-i\pi V/V_\pi} \hat{a}_{\text{in}} \approx (1 - i\pi V/V_\pi) \hat{a}_{\text{in}}, \quad (\text{A.1})$$

where V is the classical voltage applied at the input and the half-voltage V_π is the voltage at which the phase modulator applies a phase shift of π . For the quantum model, the classical fields are replaced by their quantum equivalent. The microwave input becomes $\hat{V} = \sqrt{\hbar\omega_{\text{MW}}Z_0}(\hat{b} + \hat{b}^\dagger)/\sqrt{2}$ with \hat{b} the annihilation operator for the microwave field at frequency ω_{MW} traveling on a transmission line of impedance Z_0 . The optical input is $\hat{a}_{\text{in}} = \alpha e^{-i\omega_{\text{opt}}t} + \delta\hat{a}_{\text{in}}$, where α is the amplitude of the coherent carrier field of frequency ω_{opt} , with $|\alpha|^2 = P_{\text{opt}}/\hbar\omega_{\text{opt}}$, and $\delta\hat{a}_{\text{in}}$ carries the quantum fluctuations of the input optical field. Inserting the expressions in Eq. (A.1), we can compute $\delta\hat{a}_{\text{out}} = \hat{a}_{\text{out}} - \alpha e^{-i\omega_{\text{opt}}t}$, the quantum fluctuations of the output optical field, given by

$$\delta\hat{a}_{\text{out}} = \delta\hat{a}_{\text{in}} - i\sqrt{G}e^{-i\omega_{\text{opt}}t}(\hat{b} + \hat{b}^\dagger) \quad (\text{A.2})$$

with the transduction gain G given by Eq. (3).

To understand the implications of Eq. (A.2) for the quantum noise in the transduction, we compute the

power spectral density of the output optical field,

$$\begin{aligned} \mathcal{S}_{\delta a^\dagger \delta a}^{\text{out}}[\omega_{\text{opt}} + \omega_{\text{MW}}] &= \mathcal{S}_{\delta a^\dagger \delta a}^{\text{in}}[\omega_{\text{opt}} + \omega_{\text{MW}}] \\ &+ G(\mathcal{S}_{b^\dagger b}[\omega_{\text{MW}}] + \mathcal{S}_{b b^\dagger}[-\omega_{\text{MW}}]). \end{aligned} \quad (\text{A.3})$$

The first term corresponds to the *added* quantum noise due to the input optical field. The second term contains contributions from the microwave frequency ω_{MW} , including both the signal and noise. The third term contains *added* microwave noise at frequency $-\omega_{\text{MW}}$, composed of thermal and quantum noise components, respectively $n_{\text{th}}^{\text{MW}} + 1/2$. Thus Eq. (A.3) can be simplified to

$$\begin{aligned} \mathcal{S}_{\delta a^\dagger \delta a}^{\text{out}}[\omega_{\text{opt}} + \omega_{\text{MW}}] &= \\ G \mathcal{S}_{b^\dagger b}[\omega_{\text{MW}}] + G \left(n_{\text{th}}^{\text{MW}} + \frac{1}{2} \right) + \frac{1}{2}. \end{aligned} \quad (\text{A.4})$$

We emphasize two limiting cases. When $G \ll 1$, as in our experiment, the added noise is dominated by the input optical quantum noise, the last term in Eq. (A.4). In the opposite limit, $G \gg 1$, the added noise is dominated by the microwave input noise, and the signal-to-noise ratio is independent of G . In any case, the added noise referred to the input is given by Eq. (5).

When using a quantum-limited pre-amplifiers before the electro-optical transducer, we can model the readout chain as shown in Fig. 5. The total added noise of the readout chain is

$$n_{\text{add}}^{\text{total}} = n_{\text{add}}^{\text{PA}} + \frac{n_{\text{add}}^{\text{PA}}}{G_{\text{PA}}} \simeq n_{\text{add}}^{\text{PA}} + \frac{1}{2G_{\text{PA}}G} \quad (\text{A.5})$$

Therefore when $G \simeq 1/G_{\text{PA}}$, the total added noise will be dominated by $n_{\text{add}}^{\text{PA}} = \mathcal{O}(1 \text{ quanta}/(\text{s} \cdot \text{Hz}))$ [25–28] and the readout will be near-quantum-limited.

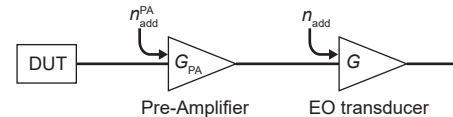


FIG. 5. Schematic signal flow when pre-amplifier is used.

Data availability statement

The code and data used to produce the plots within this paper will be available at a Zenodo open-access repository. All other data used in this study are available from the corresponding authors upon reasonable request.

ACKNOWLEDGMENTS

We thank Nils J. Engelsen for thorough reading of the manuscript. This work was supported by the European Union’s Horizon 2020 research and innovation

programme under grant agreement No. 732894 (FET Proactive HOT), and from the European Research Council (ERC) under the European Unions Horizon 2020 research and innovation programme (grant agreement No. 835329). This work was supported by funding from the

Swiss National Science Foundation under grant agreement NCCR-QSIT: 51NF40_185902 and Sinergia grant no. 186364 (QuantEOM). The circuit electro-mechanical device was fabricated in the Center of MicroNanoTechnology (CMi) at EPFL.

[1] Peter J Winzer, David T Neilson, and Andrew R Chraplyvy, “Fiber-optic transmission and networking: the previous 20 and the next 20 years,” *Optics express* **26**, 24190–24239 (2018).

[2] Christoforos Kachris and Ioannis Tomkos, “A Survey on Optical Interconnects for Data Centers,” *IEEE Communications Surveys Tutorials* **14**, 1021–1036 (2012).

[3] M. H. Devoret and R. J. Schoelkopf, “Superconducting Circuits for Quantum Information: An Outlook,” *Science* **339**, 1169–1174 (2013).

[4] John M. Martinis, Michel H. Devoret, and John Clarke, “Quantum Josephson junction circuits and the dawn of artificial atoms,” *Nature Physics* **16**, 234–237 (2020).

[5] Alexandre Blais, Steven M. Girvin, and William D. Oliver, “Quantum information processing and quantum optics with circuit quantum electrodynamics,” *Nature Physics* **16**, 247–256 (2020).

[6] A. A. Clerk, K. W. Lehnert, P. Bertet, J. R. Petta, and Y. Nakamura, “Hybrid quantum systems with circuit quantum electrodynamics,” *Nature Physics* **16**, 257–267 (2020).

[7] Ed L Wooten, Karl M Kiss, Alfredo Yi-Yan, Edmond J Murphy, Donald A Lafaw, *et al.*, “A review of lithium niobate modulators for fiber-optic communications systems,” *IEEE Journal of selected topics in Quantum Electronics* **6**, 69–82 (2000).

[8] Marian W Pospieszalski, Sander Weinreb, Roger D Norrod, and Ronald Harris, “Fets and hemts at cryogenic temperatures-their properties and use in low-noise amplifiers,” *IEEE transactions on microwave theory and techniques* **36**, 552–560 (1988).

[9] KH George Duh, Marian W Pospieszalski, William F Kopp, Pin Ho, Amani A Jabra, *et al.*, “Ultra-low-noise cryogenic high-electron-mobility transistors,” *IEEE transactions on electron devices* **35**, 249–256 (1988).

[10] S. Weis, R. Riviere, S. Deleglise, E. Gavartin, O. Arcizet, *et al.*, “Optomechanically induced transparency,” *Science* **330**, 15201523 (2010).

[11] X. Zhou, F. Hocke, A. Schliesser, A. Marx, H. Huebl, *et al.*, “Slowing, advancing and switching of microwave signals using circuit nanoelectromechanics,” *Nature Physics* **9**, 179184 (2013).

[12] Amir H Safavi-Naeini, TP Mayer Alegre, Jasper Chan, Matt Eichenfield, Martin Winger, *et al.*, “Electromagnetically induced transparency and slow light with optomechanics,” *Nature* **472**, 69–73 (2011).

[13] J. D. Teufel, Dale Li, M. S. Allman, K. Cicak, A. J. Sirois, *et al.*, “Circuit cavity electromechanics in the strong-coupling regime,” *Nature* **471**, 204208 (2011).

[14] Cheng Wang, Mian Zhang, Xi Chen, Maxime Bertrand, Amirhassan Shams-Ansari, *et al.*, “Integrated lithium niobate electro-optic modulators operating at cmos-compatible voltages,” *Nature* **562**, 101104 (2018).

[15] Yang He, Qi-Fan Yang, Jingwei Ling, Rui Luo, Hanxiao Liang, Mingxiao Li, Boqiang Shen, Heming Wang, Kerry Vahala, and Qiang Lin, “Self-starting bi-chromatic LiNbO_3 soliton microcomb,” *Optica* **6**, 1138–1144 (2019).

[16] Stefan Abel, Felix Eltes, J. Elliott Ortmann, Andreas Messner, Pau Castera, *et al.*, “Large pockels effect in micro- and nanostructured barium titanate integrated on silicon,” *Nature Materials* **18**, 4247 (2019).

[17] Felix Eltes, Gerardo E. Villarreal-Garcia, Daniele Caimi, Heinz Siegwart, Antonio A. Gentile, *et al.*, “An integrated cryogenic optical modulator,” arXiv:1904.10902 [physics] (2019), arXiv: 1904.10902.

[18] Alex I. Braginski, “Superconductor Electronics: Status and Outlook,” *Journal of Superconductivity and Novel Magnetism* **32**, 23–44 (2019).

[19] Qixiang Cheng, Meisam Bahadori, Madeleine Glick, Sébastien Rumley, and Keren Bergman, “Recent advances in optical technologies for data centers: a review,” *Optica* **5**, 1354–1370 (2018).

[20] David Thomson, Aaron Zilkie, John E Bowers, Tin Komljenovic, Graham T Reed, *et al.*, “Roadmap on silicon photonics,” *Journal of Optics* **18**, 073003 (2016).

[21] Daniel J Blumenthal, Bengt-Erik Olsson, Giammarco Rossi, Timothy E Dimmick, Lavanya Rau, *et al.*, “All-optical label swapping networks and technologies,” *Journal of Lightwave Technology* **18**, 2058 (2000).

[22] Chen Sun, Mark T Wade, Yunsup Lee, Jason S Orcutt, Luca Alloatti, *et al.*, “Single-chip microprocessor that communicates directly using light,” *Nature* **528**, 534–538 (2015).

[23] David AB Miller, “Optical interconnects to silicon,” *IEEE Journal of Selected Topics in Quantum Electronics* **6**, 1312–1317 (2000).

[24] Frank Arute, Kunal Arya, Ryan Babbush, Dave Bacon, Joseph C. Bardin, *et al.*, “Quantum supremacy using a programmable superconducting processor,” *Nature* **574**, 505–510 (2019).

[25] Tsuyoshi Yamamoto, K Inomata, M Watanabe, K Matsuba, T Miyazaki, *et al.*, “Flux-driven josephson parametric amplifier,” *Applied Physics Letters* **93**, 042510 (2008).

[26] Chris Macklin, K OBrien, D Hover, ME Schwartz, V Bolkhovsky, *et al.*, “A near-quantum-limited josephson traveling-wave parametric amplifier,” *Science* **350**, 307–310 (2015).

[27] Irfan Siddiqi, R Vijay, F Pierre, CM Wilson, M Metcalfe, *et al.*, “Rf-driven josephson bifurcation amplifier for quantum measurement,” *Physical review letters* **93**, 207002 (2004).

[28] MA Castellanos-Beltran, KD Irwin, GC Hilton, LR Vale, and KW Lehnert, “Amplification and squeezing of quantum noise with a tunable josephson metamaterial,” *Nature Physics* **4**, 929–931 (2008).

[29] Wentao Jiang, Rishi N Patel, Felix M Mayor, Timothy P McKenna, Patricio Arrangoiz-Arriola, *et al.*, “Lithium niobate piezo-optomechanical crystals,” *Optica* **6**, 845–853 (2019).

[30] Wentao Jiang, Christopher J Sarabalis, Yanni D Dahmani, Rishi N Patel, Felix M Mayor, *et al.*, “Efficient bidirectional piezo-optomechanical transduction between microwave and optical frequency,” arXiv preprint arXiv:1909.04627 (2019).

[31] John G Bartholomew, Jake Rochman, Tian Xie, Jonathan M Kindem, Andrei Ruskuc, *et al.*, “On-chip coherent microwave-to-optical transduction mediated by ytterbium in YVO_4 ,” arXiv preprint arXiv:1912.03671 (2019).

[32] A. P. Higginbotham, P. S. Burns, M. D. Urmey, R. W. Peterson, N. S. Kampel, *et al.*, “Harnessing electro-optic correlations in an efficient mechanical converter,” *Nature Physics* **14**, 10381042 (2018).

[33] Moritz Forsch, Robert Stockill, Andreas Wallucks, Igor Marinković, Claus Gärtner, *et al.*, “Microwave-to-optics conversion using a mechanical oscillator in its quantum ground state,” *Nature Physics* **16**, 69–74 (2020).

[34] G Arnold, M Wulf, S Barzanjeh, ES Redchenko, A Rueda, *et al.*, “Converting microwave and telecom photons with a silicon photonic nanomechanical interface,” arXiv preprint arXiv:2002.11628 (2020).

[35] Mankei Tsang, “Cavity quantum electro-optics,” *Physical Review A* **81**, 063837 (2010).

[36] Alfredo Rueda, Florian Sedlmeir, Michele C Collodo, Ulrich Vogl, Birgit Stiller, *et al.*, “Efficient microwave to optical photon conversion: an electro-optical realization,” *Optica* **3**, 597–604 (2016).

[37] Alfredo Rueda, Florian Sedlmeir, Madhuri Kumari, Gerd Leuchs, and Harald G. L. Schwefel, “Resonant electro-optic frequency comb,” *Nature* **568**, 378381 (2019).

[38] Linran Fan, Chang-Ling Zou, Risheng Cheng, Xiang Guo, Xu Han, *et al.*, “Superconducting cavity electro-optics: A platform for coherent photon conversion between superconducting and photonic circuits,” *Science Advances* **4** (2018), 10.1126/sciadv.aar4994.

[39] A. A. Clerk, M. H. Devoret, S. M. Girvin, Florian Marquardt, and R. J. Schoelkopf, “Introduction to quantum noise, measurement, and amplification,” *Reviews of Modern Physics* **82**, 1155–1208 (2010).

[40] Christian Herzog, Gorazd Poberaj, and Peter Gnter, “Electro-optic behavior of lithium niobate at cryogenic temperatures,” *Optics Communications* **281**, 793796 (2008).

[41] Jeffrey D. Morse, Kent George McCammon, Charles F. McConaghy, Don A. Masquelier, Henry E. Garrett, *et al.*, “Characterization of lithium niobate electro-optic modulators at cryogenic temperatures,” in *Design, Simulation, and Fabrication of Optoelectronic Devices and Circuits*, Vol. 2150, edited by Mario Nicola Armenise, International Society for Optics and Photonics (SPIE, 1994) pp. 283–291.

[42] C. McConaghy, M. Lowry, R.A. Becker, and B.E. Kincaid, “The performance of pigtailed annealed proton exchange linbo 3 modulators at cryogenic temperatures,” *IEEE Photonics Technology Letters* **8**, 14801482 (1996).

[43] K. Yoshida, Y. Kanda, and S. Kohjiro, “A traveling-wave-type linbo/sub 3/ optical modulator with superconducting electrodes,” *IEEE Transactions on Microwave Theory and Techniques* **47**, 12011205 (1999).

[44] Shoko Ohteru and Noboru Takachio, “Optical signal quality monitor using direct q-factor measurement,” *IEEE Photonics Technology Letters* **11**, 1307–1309 (1999).

[45] Ippei Shake, Hidehiko Takara, and Satoki Kawanishi, “Simple measurement of eye diagram and ber using high-speed asynchronous sampling,” *Journal of lightwave technology* **22**, 1296 (2004).

[46] J. D. Teufel, T. Donner, Dale Li, J. W. Harlow, M. S. Allman, *et al.*, “Sideband cooling of micromechanical motion to the quantum ground state,” *Nature* **475**, 359363 (2011).

[47] E. E. Wollman, C. U. Lei, A. J. Weinstein, J. Suh, A. Kronwald, *et al.*, “Quantum squeezing of motion in a mechanical resonator,” *Science* **349**, 952955 (2015).

[48] CF Ockeloen-Korppi, E Damskägg, J-M Pirkkalainen, M Asjad, AA Clerk, *et al.*, “Stabilized entanglement of massive mechanical oscillators,” *Nature* **556**, 478–482 (2018).

[49] Shabir Barzanjeh, ES Redchenko, Matilda Peruzzo, Matthias Wulf, DP Lewis, *et al.*, “Stationary entangled radiation from micromechanical motion,” *Nature* **570**, 480–483 (2019).

[50] N. R. Bernier, L. D. Tth, A. Koottandavida, M. A. Ioannou, D. Malz, *et al.*, “Nonreciprocal reconfigurable microwave optomechanical circuit,” *Nature Communications* **8** (2017), 10.1038/s41467-017-00447-1.

[51] L. D. Tth, N. R. Bernier, A. Nunnenkamp, A. K. Fedorov, and T. J. Kippenberg, “A dissipative quantum reservoir for microwave light using a mechanical oscillator,” *Nature Physics* **13**, 787793 (2017).

[52] Markus Aspelmeyer, Tobias J Kippenberg, and Florian Marquardt, “Cavity optomechanics,” *Reviews of Modern Physics* **86**, 1391 (2014).

[53] Florian Marquardt, JGE Harris, and Steven M Girvin, “Dynamical multistability induced by radiation pressure in high-finesse micromechanical optical cavities,” *Physical Review Letters* **96**, 103901 (2006).

[54] Tal Carmon, Hossein Rokhsari, Lan Yang, Tobias J Kippenberg, and Kerry J Vahala, “Temporal behavior of radiation-pressure-induced vibrations of an optical microcavity phonon mode,” *Physical Review Letters* **94**, 223902 (2005).

[55] D Cattiaux, X Zhou, S Kumar, I Golokolenov, RR Gazizulin, *et al.*, “Beyond linear coupling in microwave optomechanics,” arXiv preprint arXiv:2003.03176 (2020).

[56] Cheng Wang, Mian Zhang, Xi Chen, Maxime Bertrand, Amirhassan Shams-Ansari, *et al.*, “Integrated lithium niobate electro-optic modulators operating at cmos-compatible voltages,” *Nature* **562**, 101–104 (2018).

[57] Sasikanth Manipatruni, Kyle Preston, Long Chen, and Michal Lipson, “Ultra-low voltage, ultra-small mode volume silicon microring modulator,” *Optics express* **18**, 18235–18242 (2010).

[58] J Elliott Ortmann, Felix Eltes, Daniele Caimi, Norbert Meier, Alexander A Demkov, *et al.*, “Ultra-low-power tuning in hybrid barium titanate–silicon nitride electro-optic devices on silicon,” *ACS Photonics* **6**, 2677–2684 (2019).